Theoretical investigation on mechanism and kinetics of M2CAA initiated by Cl atom in the atmosphere

Original Research Article

ABSTRACT

A comprehensive theoretical investigation was conducted to elucidate the mechanism, kinetics, and thermochemistry of the gas-phase reactions between Methyl 2-chloroacetoacetate ($CH_3C(O)CHClC(O)OCH_3$, M2CAA) and Chlorine atoms using the M06-2X functional. The most thermodynamically stable conformer of M2CAA was identified at ambient temperature. Three primary hydrogen abstraction pathways were characterized, each proceeding through the formation of a pre-reactive complex, indicating that the reactions follow an indirect hydrogen abstraction mechanism. Rate coefficients for these pathways were calculated for the first time over a temperature range of 250–450 K using Canonical Transition State Theory (CTST). Based on these kinetic results, the atmospheric lifetime of M2CAA was estimated to be approximately 1.85 days. From these results, it can be emphasize that the hydrogen abstraction from the –CHCl group is kinetically more advantageous than the other two reaction pathways i.e. abstraction from $–CH_3$ and $– COOCH_3$ group.

Keywords: Chloroacetoacetate, DFT, IRC calculation, Rate constant, Atmospheric lifetime

INTRODUCTION

In recent decades, it has been stated that volatile organic compounds (VOCs), most likely hydrofluoroethers (HFEs), are widely acknowledged and recommended as a third-generation alternative to hydrofluorocarbons (HFCs), hydrochlorofluorocarbons (HCFCs), and chlorofluorocarbons (CFCs). These substances are used in refrigerator heat transfer fluid, foam blowing agents, lubricant deposition, and electronic equipment cleaning [1–3]. The primary mechanisms for HFE degradation in the atmosphere may be initiated in coastal locations by reactions with OH radicals and Cl atoms, as well as possibly with aerosols containing chloride from highly mechanized metropolitan areas.

Solvents, fuel additives, and cleaning and disinfection chemicals are all made with oxygenated volatile organic compounds, (OVOCs.) These substances can primarily undergo chemical transformations when released into the atmosphere, producing reaction products that may be more dangerous than the precursors [4,5]. OH radical-initiated photo oxidation processes are the primary pathway for OVOC oxidation in the troposphere [6,7]. The family of Oxygenated Volatile Organic Compounds (OVOCs) known as carbonyl esters includes methyl 2-chloroacetoacetate (M2CAA) and ethyl 2-chloroacetoacetate (E2CAA) [8]. These VOCs have an oxygen bond that increases the reactivity of the molecule's neighboring hydrogen atoms to tropospheric oxidants like photolysis or OH or Cl radicals. Acetates have been widely released into the atmosphere as a result of industrial activity; these oxygenated volatile organic compounds will react with the primary tropospheric oxidants [9,10].

Chemical transformation is the primary determinant of these chemicals' destiny in the atmosphere. The primary cleaner in the marine boundary layer, chlorine atoms are crucial to the breakdown of OVOCs-initiated photo oxidation processes, which are brought on by the addition of a double bond or by mechanisms of hydrogen atom abstraction [11]. Similarly, larger

concentrations of Cl atoms, which can reach 1×10^5 atoms cm^{-3} or more, in marine or heavily industrialized [12] environments may result in competitive interactions with the OH radical that triggered the breakdown of these VOCs [13].

Certain OVOCs, such as chloroacetoacetates, which are commonly employed as anti-slime antimicrobial and pesticide agents to eradicate slime-producing microorganisms such algae, fungi, and slime molds on pools, are released by the paper industry. These substances can be transmitted to water reservoirs or evaporate into the atmosphere if they are often used as insecticides. Instead of dry and wet deposition, chemical transformation is the primary determinant of the sink of OVOCs, such as esters and haloesteres. Methyl 2-chloroacetoacetate was used in one-pot synthesis of 2-arylimidazole-4-carboxylic acidsand 3,5-disubstituted 1,2,4-triazoles [14,15]. To ascertain their environmental impact on the quality of air and other matrices, kinetic and mechanistic analyses of the degradation of chloroacetoacetates triggered by interaction with Cl radicals are pertinent. A well-defined theoretical study is very desirable in order to identify the feasible mechanism and gain a better grasp of the kinetics of the title reaction. In order to gain a more thorough knowledge of the title reaction, we presented a thorough theoretical analysis of the hydrogen abstraction reaction between M2CAA and Cl radical as an addition to the experiments.

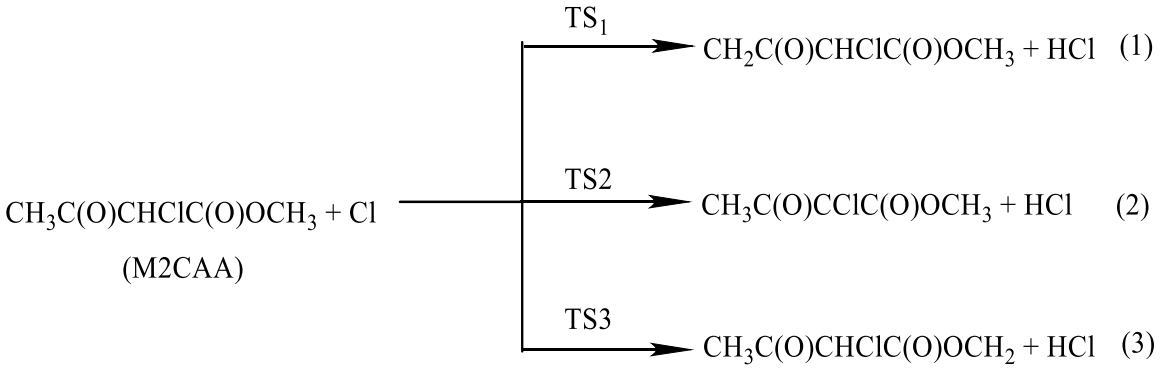

However, there has only been one experimental research project on kinetic of M2CAA + Cl reaction as far as we know. Recently, Vianni et al. [16] reported the Rate coefficients for the

gas-phase reactions of Cl radical with M2CAA using the relative technique with different reference compounds. They reported a rate constant value as $(2.54 \pm 0.81) \times 10^{-10}$ cm^3 $molecule^{-1}$ s^{-1}at (298 ± 2) K. It has been also reported that by employing structure activity relationship (SAR) method, Aschmann and Atkinson [17] estimated rate coefficients for the reactions of M2CAA with Cl atoms. The SAR value for the reaction of M2CAA with chlorine atoms is established to be 3.68×10^{-11} cm^3 $molecule^{-1}$ s^{-1}. As far as we are aware, this is the first thorough theoretical investigation of M2CAA's H-abstraction interactions with Cl radical. We think that our work will be helpful for a better understanding of this significant reaction, since experimental study mainly provides just the overall rate constant.

COMPUTATIONAL METHODS

We performed all the computational quantum calculations work using Gaussian 09 program package [18]. The electronic structures of the reactants (Rs), reaction complexes (RCs), product complexes (PCs), transition states (TSs) and products (Ps) were optimized using hybrid density functional M06-2X [19] along with 6-31+G(d,p) basis set. Further, we were carried out frequency calculations of all the optimized species using the same M06-2X /6-31+G(d,p) method. From frequency analysis, we found that for stable species, these were no imaginary frequencies which ensure these molecules to have either local or global minima energies while for the TSs, we found one imaginary frequency to ensure it has maxima along the reaction coordinate. Previous reports [20–25] have demonstrated that this hybrid density functional, M06-2X, produces satisfactory results for thermochemistry and kinetics for the hydrogen abstraction reactions for the volatile organic compounds. In order to validate to correct TSs which was really connecting the reactant and product species, we performed IRC calculation [26] throughout the reaction channels.

RESULTS AND DISCUSSION

We first identified the most stable M2CAA conformers using scan calculations, and we then chose the most stable conformer for further study. For the hydrogen abstraction reactions, we have considered three reaction routes (1-3), mainly hydrogen abstraction from the $–CH_3$ group, –CHCl group, and $–COOCH_3$ group. It can be seen from the geometrical parameters and stereographical orientation, the hydrogen atoms in the $–CH_3$ group and $–COOCH_3$ groups are not equivalent. The stereographic environment of one H-atom (C7-H8) is different from the other two (C7-H9 and C7-H10) in the $–CH_3$ group as shown in Fig.1. Therefore, two transition states should be located for reaction channels 1 and 3. However, only one transition state could be located for hydrogen abstraction from the $–CH_3$ group and $–COOCH_3$ groups. Therefore, we have presented only one reaction channel each for reactions 1 and 3. Thus, we have located three transition states namely TS1, TS2 and TS3, respectively for three reaction channels (1 – 3). Pre-reactive complexes (RC1, RC2, and RC3) have been found in the entrance channel for reactions (1-3) in the current investigation. The exit channel also contains product complexes, referred to as PC1, PC2 and PC3, with energies lower than the corresponding products before the final product is distributed. Therefore, it is clear that the reaction channels (1-3) may employ indirect procedures. The least energy path was used to find stationary spots on a relaxed potential energy surface. Figs. 1 and 2 show the electronic structure of the optimized geometry of the reactant, products, reaction complexes, product complexes, and transition states that were produced at the M06-2X/6-31+G(d,p) level.

At the M06-2X/6-31+G(d,p) level, the precise thermodynamic calculations for reaction enthalpies (Δ_rH°) and free energies (Δ_rG°) at 298 K for loss processes (1–3) are documented in Table 1. These thermodynamic functions were determined with thermal corrections to the energy at 298 K. The calculated $\Delta_rH°$ and $\Delta_rG°$ values at 298 K indicate that the decomposition

pathways taken into consideration in this investigation are feasible and spontaneous. It is evident from Table 1 that the reaction channel 2 is more thermodynamically viable. Because $\Delta_r H^\circ_{298} > 0$, the results also show that reaction channels 1& 2 are exothermic in nature while reaction channel 3 is endothermic in nature.

The C–H bond of the departing hydrogen and the newly generated bond between the H and Cl atom are crucial structural characteristics that must be monitored throughout the development of transition states. The breaking C–H bond length is 25.87% greater than the observed C–H bond length in the isolated M2CAA molecule, while the forming H...Cl bond length is 19.5% longer than the H–Cl bond length in isolated HCl molecule, according to a visualization of the optimized structures of TS1 for reaction 1. This implies that the barrier of the reaction 1 is closer to the product, and that the reactions with Cl atoms proceed via late transition state which is in consonance with Hammond's postulate [27]. Similarly, for transition state TS2 for reaction 2, the length of the breaking C-H bond (C15-H12) is found to be longer by 17.56% than the observed C-H bond length in isolated M2CAA molecule whereas the forming H...Cl bond length is longer by 21.48% than the H-Cl bond length in isolated HCl molecule. This implies that the barrier of the reaction 2 is closer to the reactant, and that the reactions with Cl atoms proceed via early transition state. Visualization of the optimized structures of TS3 for reaction 3 reveals that the length of the broken C-H bond (C3 –H6) is 29.77% longer than the C–H bond length that was determined in the isolated M2CAA molecule.

Table 2 presents the results of the harmonic vibrational frequency calculation at the M06-2X/6-31+G(d,p) level. Each transition state has one imaginary frequency due to its first order saddle point character, while the analysis of the harmonic vibrational frequency of minima including reactants, reactant complexes (RCs), product complexes (PCs), and products (P1 and P2) revealed no imaginary frequency (NIMAG = 0). The Cl7–H8 and C7–H8 stretching modes

are represented by the imaginary frequency of TS1 for reaction channel (1), which is 1115 cm^{-1}. This also shows a considerable curvature in the potential energy surface (PES) surrounding the transition state. The imaginary frequency for the hydrogen abstraction from the –CHCl group involving TS2 is determined to be –1010 cm^{-1}, which corresponds to the stretching modes for hydrogen transfer reactions Cl17–H12 and C15–H12. At the M06-2X/6-31+G(d,p) level, the transition states TS3 for hydrogen abstraction from the $–COOCH_3$ group were optimized with a single imaginary frequency, which was found to be –816 cm^{-1}.

The representation of the normal-mode corresponding to the calculated imaginary frequencies shows a clear transition state geometry connecting reactants and products during transition. To further ascertain whether a transition state exists on the potential energy surface, the intrinsic reaction coordinate (IRC) calculation [26] is performed at the same theoretical level using the Gonzalez-Schlegel steepest descent path in the mass-weighted Cartesian coordinates with a step size of 0.01($amu^{1/2}$- bohr). Additional proof that the transition state truly connects the intended reactant and product along the corresponding potential energy surface is given by the results of IRC calculations, which are shown in Fig. 3. Table 3 summarizes the energy of each optimized geometry used in this study, which was determined using the M06-2X/6-311++G(d,p) method. We employed the species' optimal geometries, M06-2X/6-31+G(d,p), for the energetic computation. Using frequency calculation data at the M06-2X/6-31+G(d,p) level of theory, optimization was carried out to find each species' zero-point energy. Zero-point energy (ZPE) corrected total energies were calculated with a scale factor of 0.967 [28]. The total energy of the reactants R + Cl, (M2CAA + Cl) is set to be zero for reference, and the values in parentheses are relative energies in kcal mol^{-1} with reference to reactants. Fig. 4 shows a schematic potential energy profile of M2CAA reactivity with Cl atom that was acquired at the M06-2X level using zero-point energy (ZPE) adjustments. Zero-point energy corrected total

energy has been used in the energy diagram's development. For TS1, TS2, and TS3, the energy barrier determined at the M06-2X/6-31+G(d,p) level is 1.65, –0.78, and 0.62 kcal mol^{-1}, respectively. The barrier height values suggest that hydrogen abstraction by Cl atom from the –-CHCl group of M2CAA is more facile than that from the $–CH_3$ or $–COOCH_3$ group.

KINETICS CALCULATION

The conventional transition state theory (CTST) [29] and Eckart's tunneling correction [30] were used to calculate the rate coefficient values for various reaction channels spanning the 250–450 K temperature range using the following formula.

$$k = \sigma \Gamma(T) \frac{k_B T}{h} \frac{Q^{\ddagger}_{TS}}{Q_R} \exp \frac{-\Delta E}{RT} \qquad (4)$$

The σ represents symmetry factor whereas tunneling correction factor at temperature T is represented by the symbol Γ(T). The total partition functions (per unit volume) for the reactants and transition states are denoted by Q_R and $Q^{\ddagger}_{TS}$,, respectively. R stands for the universal gas constant, k_B for the Boltzmann constant, h for Planck's constant, and ΔE for the barrier height incorporating zero point energy correction. In present work, the kinetic rate coefficients for reaction pathways (1–3) were performed by means of the Kinetic and Statistical Thermodynamical Package (KiSThelP) programme [31]. The obtained rate coefficients in the temperature range of 250 – 450 K for reaction pathways (1–3) are recorded in Table 4. At 298 K, our calculated rate constants for TS1, TS2, and TS3 were found to be 7.83×10^{-13} , 1.17×10^{-11} and 6.40×10^{-12} cm^3 $molecule^{-1}$ s^{-1} respectively at M06-2X/6-31+G(d,p) level of theory. The computed overall k_{Cl} value for M2CAA with Cl atom reaction using the M06-2X barrier height is found to be 1.90×10^{-11} cm^3 $molecule^{-1}$ s^{-1} at 298 K. Our calculated rate constant for the reaction of M2CAA with Cl atom is in good agreement with the reported SAR value of 3.68 ×

10^{-11} cm^3 $molecule^{-1}$ s^{-1} [17]. However, our calculated value is slightly lower than the value of rate constant (2.16 ± 0.85) $\times 10^{-10}$ cm^3 $molecule^{-1}$ s^{-1} at (298 ± 2) K by Vianni et al. [16]. The percentage branching ratios for each of the reaction channels determined at 298 K are found to be 4.14, 62.10 and 3376 %, respectively. From these results, it can be emphasize that the hydrogen abstraction from the –CHCl group is kinetically more advantageous than the other two reaction pathways i.e. abstraction from $–CH_3$ and $– COOCH_3$ group.

ATMOSPHERIC LIFETIME

In general, tropospheric lifetime (τ_{eff}) of M2CAA can be estimated by assuming that its removal from troposphere occurs only through the reactions with Cl atoms. Then (τ_{eff}) can be expressed as [32],

$$\tau_{eff} = \tau_{Cl} \qquad (4)$$

where, $\tau_{Cl} = (k_{Cl} \times [Cl])^{-1}$. Using the 298 K value of $k_{Cl} = 1.90\times10^{-11}$ cm^3 $molecule^{-1}$ s^{-1} and the global average atmospheric Cl concentrations of 3.3×10^4 molecule cm^{-3} [33], the estimated atmospheric lifetime of M2CAA is found to be 1.85 days which is in good agreement with the reported value of 1.57 days by Vianni et al. [16].

CONCLUSIONS

In this study we have explored the atmospheric and environmental consequence of M2CAA molecule initiated by Cl atom by employing M06-2X/6-31+G(d,p) level of theory. We have done various inquires involving the optimization of structural parameters, energy profiles, thermochemistry and kinetics of the M2CAA with Cl radical. For that, we have identified three reaction channels which follow an indirect path through the formation of pre- and post- reaction complexes on the potential energy surface. In this manuscript, we applied an effective as well as reliable computational strategy for predicting accurately the tropospheric reactivity of the titled molecule and atmospheric implications. All rate constants, computed by canonical transition

state theory. The rate coefficients for the M2CAA with Cl atom, manifests positive temperature influence at 250–450 K and the rate constant at 298 K is found to be 3.68×10^{-11} cm^3 $molecule^{-1}$ s^{-1} which is in reasonable agreement with the limited experimental data. The atmospheric lifetime for M2CAA molecule is estimated to be 1.85 days. From our theoretical study along with experimental evidence it can be concluded that hydrogen abstraction from –CHCl group is more facile than that from methyl group.

REFERENCES

[1] Molina MJ, Rowland FS (1974) Nature 249:810-812

[2] Sekiya A, Misaki S (2000) J Fluorine Chem 101:215–221

[3] Powell RL (2002) J Fluorine Chem 114:237-250

[4] Zhou S, Barnes I, Zhu T, Klotz B, Albu M, Bejan I, Benter T (2006) Environ Sci Technol 40: 5415e5421

[5] Christensen LK, Ball JC, Wallington TJ (2000) J Phys Chem 104:351-354

[6] Han L, Siekmann F, Zetzsch C (2018) Atmosphere 9:320

[7] Bouzidi H, Aslan L, Dib GE, Coddeville P, Fittschen C, Tomas A (2015) Environ Sci Technol 49:12178e12186

[8] DeMore WB, Howard CJ, Sander SP, Ravishankara AR, Golden DM, Kolb CE, Hampson RF, Molina MJ, Kurylo MJ (1997) Evaluation, Vol. 4. NASA. JPL Publication

[9] Blanco MB, Barnes I, Wiesen P, Teruel MA (2016) RSC Advances 6:51834e51844

[10] Bravo I, Diaz-de-Mera Y, Aranda A, Moreno E, Nutt DR, Marston G (2011) Phys Chem Chem Phys 13:17185-17193

[11] Atkinson R, Baulch DL, Cox RA, Hampson RFJ, Kerr JA, Rossi MJ, Troe J (1997) J Phys Chem Ref Data 26:521–1011

[12] Blanco MB, Bejan I, Barnes I, Wiesen P, Teruel MA (2012) Environ Sci Technol 46: 8817e8825

[13] Blanco MB, Bejan I, Barnes I, Wiesen P, Teruel MA (2010) Environ Sci Technol 44:2354-2359

[14] Yoburn JC, Baskaran S (2005) Org Lett 7:3801-3803

[15] Tseng WC, Wang LY, Wu TS, Wong FF (2011) Tetrahedron 67:5339-5345

[16] Straccia VGC, Lugo PL, Rivela CB, Blanco MB, Teruel MA (2023) Atoms Environ 309:119925

[17] Aschmann SM, Atkinson R (1995) Int J Chem Kinet 27:613–622

[18] Frisch M J *et al*. Gaussian 09 (Revision B.01); Gaussian Inc.; Wallingford, CT, 2009.

[19] Zhao Y, Truhlar DG (2008) Theor Chem Acc 120:215-241

[20] Gour NK, Borthakur K, Paul S, Deka RC (2020) Chemosphere 238:124556

[21] Lily M, Mishra BK, Chandra AK (2014) J Fluor Chem 161:51-59

[22] Rao PK, Deka RC, Gour NK, Gejji SP (2018) J Phys Chem A 122:6799–6808

[23] Baidya B, Lily M, Patgiri D, Hynniewta S, Chandra AK (2020) New J Chem 44:4276-4284

[24] Paul S, Mishra BK, Baruah SD, Deka RC (2020) Env Sci Poll Res 27:907-920

[25] Gour NK, Mishra BK, Sarma PJ, Begum P, Deka RC (2017) J Fluor Chem 204:11–17

[26] Gonzalez C, Schlegel HB (1989) J Chem Phys 90: 2154-2161

[27] Hammond GS (1955) J Am Chem Soc 77: 334-338

[28] Alecu IM, Zheng J, Zhao Y, Truhlar DG(2010) J Chem Theory Comput 6:2872-2887

[29] Laidler KJ (2004) Chemical Kinetics, 3rd edn. Pearson Education, New Delhi

[30] Xiao R, Noerpel M, Luk HL, Wei Z, Spinney R(2014) Int J Quant Chem114:74–83

[31] Canneaux S, Boh F, Henon E (2014) J Compu. Chem 35:82-93

[32] Kurylo MJ, Orkin VL (2003) Chem Rev 103:5049-5076

[33] OW Wingenter, MK Kubo, NJ Blake, TW Smith, DR Blake, FS Rowland (1996) J Geophys Res 101: 4331-4340

Table 1 Thermochemical data (kcal mol^{-1}.) for reaction channels (1–3) calculated at M06-2X/6-31+G(d,p) level of theory at 298 K.

Reaction channels	$\Delta_r H°_{298}$	$\Delta_r G°_{298}$
Reaction 1	–4.54	–36.29
Reaction 2	–11.72	–44.07
Reaction 3	0.17	–32.58

Table 2 Harmonic vibrational frequencies of reactants, transition states and products at M06-2X/6-31+G(d,p) level of theory.

Species	Vibrational Frequencies (cm^{-1})
$CH_3C(O)CHClC(O)OCH_3$ (M2CAA)	32, 64, 88, 104, 170, 182, 205, 243, 313, 343, 408, 498, 568, 681, 766, 798, 906, 942, 1015, 1034, 1079, 1182, 1184, 1214, 1236, 1281, 1366, 1403, 1470, 1479, 1486, 1499, 1508, 1866, 1898, 3079, 3092, 3131, 3155, 3179, 3195, 3211
TS1	1115i, 14, 35, 62, 86, 90, 143, 181, 201, 242, 313, 330, 372, 400, 437, 524, 577, 685, 775, 803, 896, 925, 950, 979, 1027, 1076, 1138, 1185, 1203, 1219, 1240, 1296, 1368, 1451, 1488, 1501, 1505, 1805, 1900, 3095, 3142, 3154, 3181, 3222, 3263
TS2	1010i, 28, 65, 73, 82, 111, 121, 158, 166, 194, 229, 277, 336, 359, 430, 510, 562, 690, 775, 809, 896, 941, 988, 1019, 1055, 1084, 1114, 1187, 1220, 1235, 1345, 1409, 1471, 1479, 1488, 1501, 1506, 1852, 1885, 3085, 3097, 3163, 3188, 3199, 3216,
TS3	816i, 14, 34, 44, 70, 118, 160, 189, 220, 244, 338, 357, 387, 417, 491, 521, 568, 706, 734, 772, 879, 912, 955, 981, 999, 1043, 1190, 1203, 1225, 1243, 1254, 1303, 1308, 1405, 1467, 1471, 1479, 1874, 1907, 3079, 3145, 3154, 3155, 3197, 3288
RC1	26, 32, 66, 76, 101, 123, 159, 173, 186, 213, 244, 324, 355, 414, 496, 567, 705, 742, 777, 897, 925, 999, 1044, 1107, 1186, 1200, 1225, 1252, 1308, 1359, 1405, 1471, 1481, 1489, 1497, 1507, 1868, 1883, 3075, 3094, 3144, 3150, 3182, 3194, 3212,
RC2	29, 37, 57, 72, 99, 117, 141, 160, 189, 208, 242, 314, 343, 406, 502, 568, 677, 766, 798, 905, 942, 1014, 1037, 1078, 1183, 1185, 1214, 1238, 1286, 1371, 1404, 1470, 1480, 1487, 1497, 1506, 1871, 1897, 3085, 3096, 3130, 3159, 3182, 3202, 3218
RC3	18, 28, 60, 81, 111, 127, 154, 176, 189,219, 250, 315, 345, 411, 498, 572, 680, 767, 801, 910, 946, 1015, 1038, 1077, 1183, 1185, 1217, 1241, 1283, 1377, 1406, 1472, 1484, 1487, 1495, 1508, 1848, 1872, 3080, 3096,3133, 3154, 3186, 3201, 3214
PC1	34, 44, 52, 93, 103, 132, 186, 189, 213, 244, 314, 368, 407, 420, 427, 502, 565, 568, 735, 763, 803, 845, 932, 962, 1023, 1068, 1188, 1210, 1241, 1262, 1320, 1398, 1483, 1495, 1503, 1506, 1632, 1844, 2699, 3103, 3162, 3191, 3213, 3227, 3334
PC2	16, 41, 63, 101, 118, 146, 167, 178, 197, 240, 269, 320, 363, 402, 427, 466, 500, 563, 607, 746, 799, 962, 1003, 1029, 1053, 1140, 1185, 1226, 1304, 1341, 1405, 1471, 1479, 1487, 1496, 1501, 1738, 1829, 2785, 3085, 3096, 3158, 3183, 3205, 3223

PC3	16, 44, 47, 75, 96, 133, 156, 171, 208, 242, 312, 342, 355, 400, 419, 433, 500, 569, 672, 701, 746, 776, 885, 923, 1002, 1044, 1190, 1206, 1225, 1250, 1306, 1323, 1405, 1471, 1472, 1483, 1864, 1892, 2819, 3081, 3143, 3155, 3199, 3210, 3362
$CH_2C(O)CHClC(O)OCH_3$ (P1)	42, 81, 101, 168, 185, 200, 241, 315, 353, 410, 432, 523, 589, 687, 776, 784, 856, 918, 956, 1035, 1078, 1180, 1196, 1217, 1237, 1319, 1369, 1484, 1490, 1499, 1507, 1676, 1898, 3090, 3136, 3177, 3209, 3225, 3346
$CH_3C(O)CClC(O)OCH_3$ (P2)	22, 55, 127, 175, 182, 227, 253, 284, 325, 363, 408, 464, 569, 620, 741, 807, 955, 1007, 1033, 1050, 1156, 1187, 1231, 1277, 1359, 1405, 1467, 1481, 1487, 1495, 1509, 1746, 1822, 3087, 3095, 3168, 3182, 3195, 3213
$CH_3C(O)CHClC(O)OCH_2$ (P3)	29, 62, 84, 118, 186, 203, 239, 316, 328, 355, 419, 485, 496, 567, 672, 757, 794, 903, 934, 1017, 1034, 1133, 1192, 1209, 1248, 1282, 1352, 1402, 1469, 1471, 1478, 1868, 1903, 3079, 3133, 3155, 3197, 3233, 3390
HCl	3033

Table 3 Relative energies (in kcal mol^{-1}) with zero-point energy correction for the reactants, reaction complexes, transition states, product complexes and products at M06-2X/6-31+G(d,p) level of theory.

Species	**M06-2X/6-31+G(d,p)**
M2CAA+ Cl	0.00
RC1	–5.29
RC2	–4.67
RC3	–3.77
TS1	1.65
TS2	–0.78
TS3	0.62
PC1	-9.84
PC2	-18.67
PC3	-2.51
P1 + HCl	-4.92
P2 + HCl	-10.46
P3 + HCl	-0.19

Table 4: Rate constants of different reaction channels and overall rate constant (in cm^3 $molecule^{-1}$ s^{-1}) within the temperature range of 250–450 K at M06-2X/6-31+G(d,p) level of theory.

Rate constant	**250 K**	**298.15 K**	**300 K**	**350 K**	**400 K**	**450 K**
k_{1a}	3.84×10^{-13}	7.83×10^{-13}	8.02×10^{-13}	1.39×10^{-12}	2.14×10^{-12}	3.03×10^{-12}
k_2	1.27×10^{-11}	1.17×10^{-11}	1.17×10^{-11}	1.13×10^{-11}	1.12×10^{-11}	1.13×10^{-11}
k_{3a}	4.37×10^{-12}	6.40×10^{-12}	6.48×10^{-12}	8.54×10^{-12}	1.12×10^{-12}	1.38×10^{-11}
K_{total}	1.75×10^{-11}	**1.90×10^{-11}**	1.9×10^{-11}	2.16×10^{-11}	2.47×10^{-11}	2.82×10^{-11}

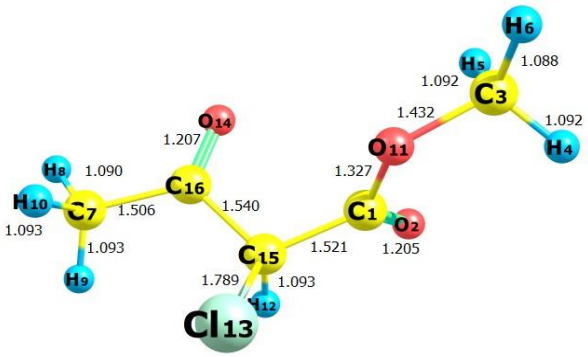

M2CAA

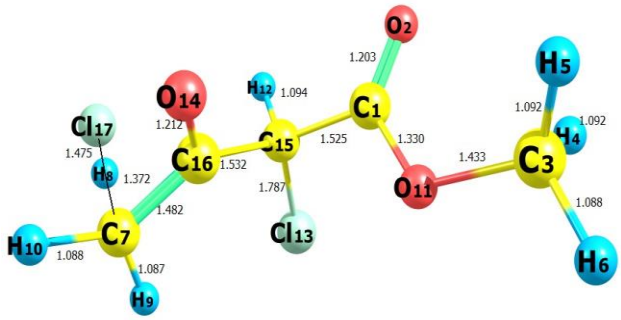

TS1

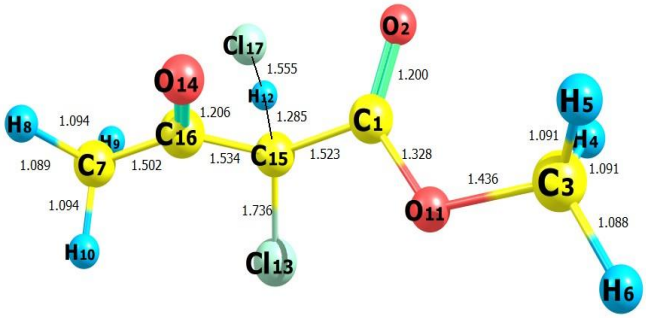

TS2

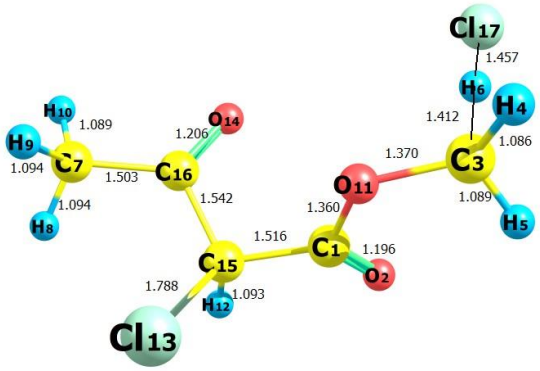

TS3

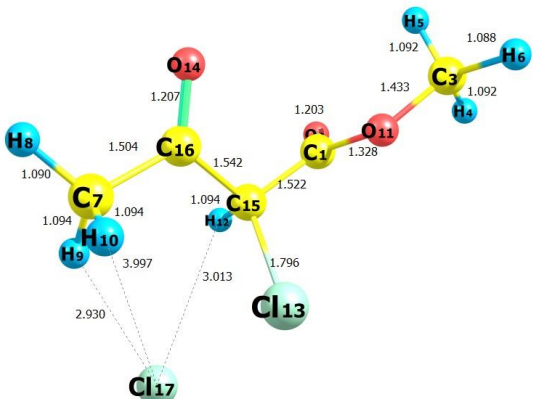

RC1

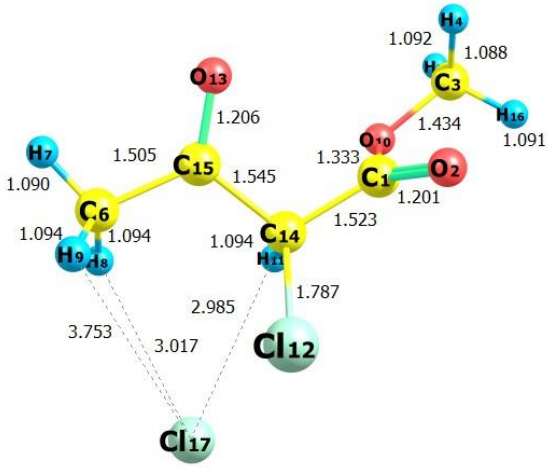

RC2

Fig. 1: Optimized geometries of M2CAA, transition states and reactive complexes at M06-2X/6-31+G(d,p)level.Bond lengths are in Angstroms.

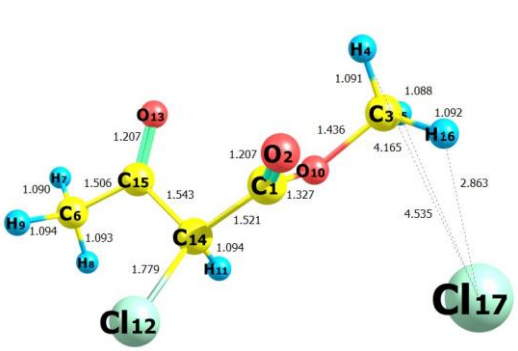

RC3

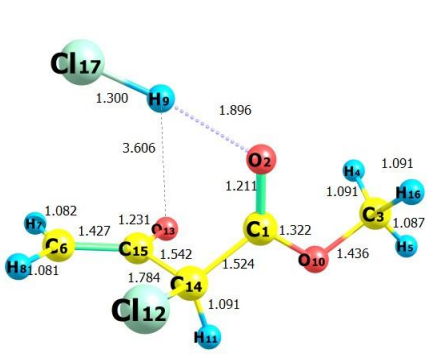

PC1

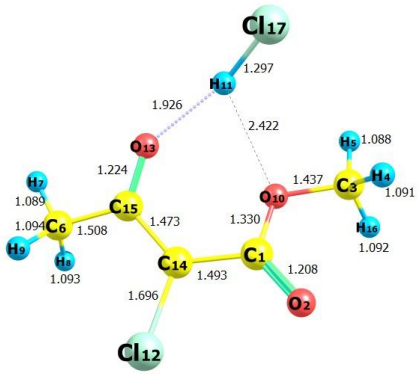

PC2

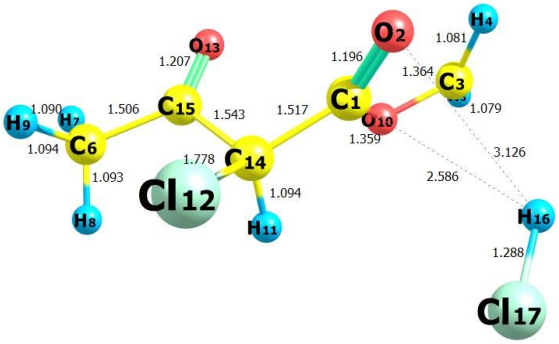

PC3

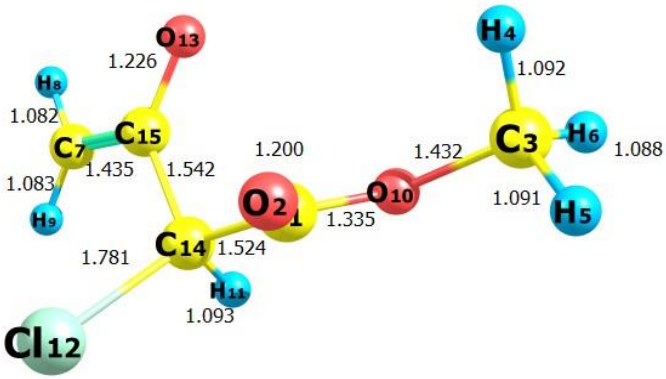

P1

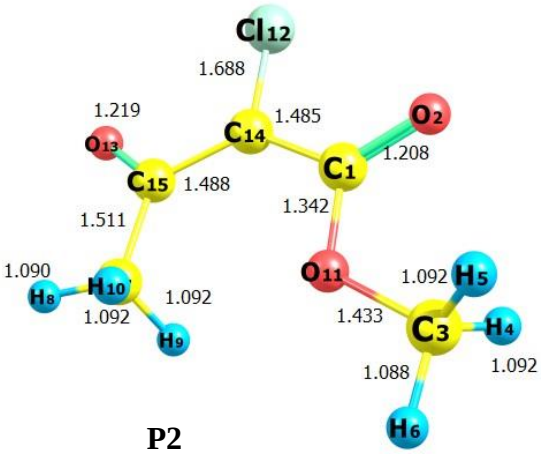

P2

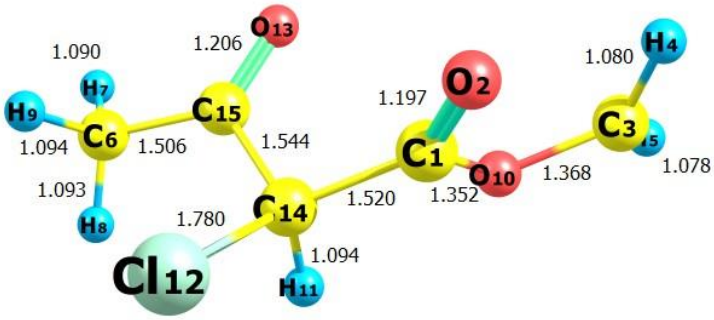

P3

Fig. 2: Optimized geometries of product complexes and products at M06-2X/6-31+G(d,p)

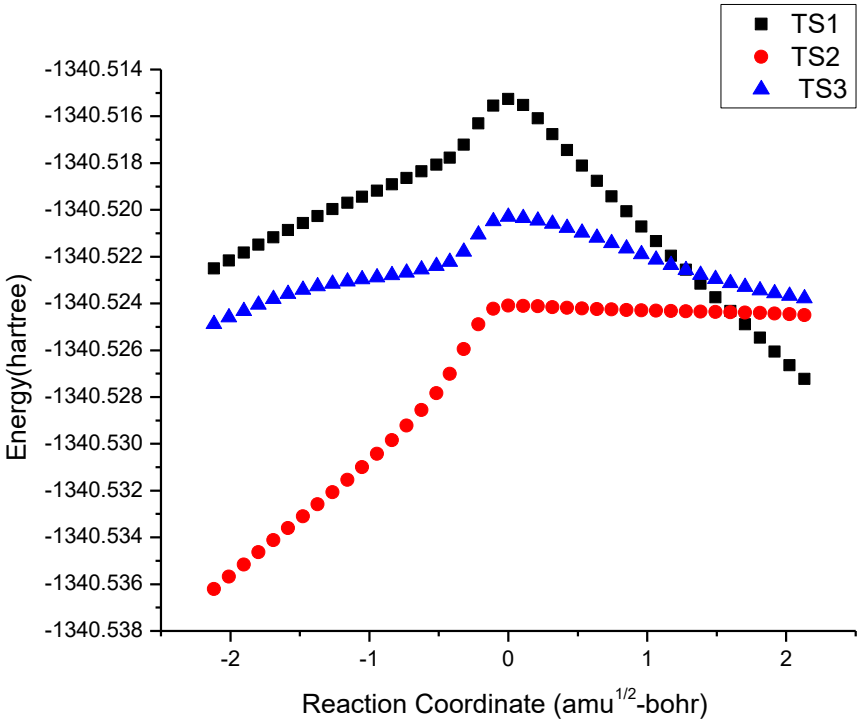

Fig. 3: IRC plot performed for transition states TS1, TS2 and TS3 for reaction channels (1-3) at M06-2X/6-31+G(d,p) level of theory.

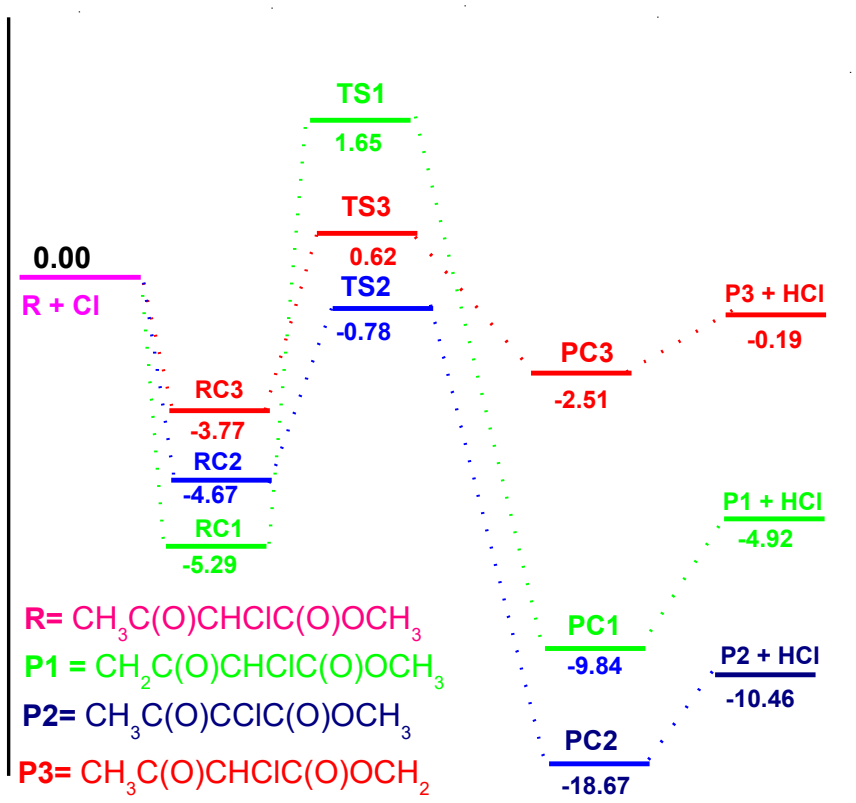

Fig. 4: Schematic potential energy diagram for the M2CAA + Cl reactions. Relative energies (in kcal mol^{-1}) with ZPE at M06-2X/6-31+G(d,p) level.